frontiers | Frontiers in Earth Science

TYPE Original Research
PUBLISHED 05 April 2023
DOI 10.3389/feart.2023.1124860

OPEN ACCESS

EDITED BY
Fei Xue,
Hohai University, China

REVIEWED BY
Jingyi Wang,
China University of Geosciences, China
Xinkai Hu,
Ministry of Natural Resources, China
Xiaofang He,
China University of Mining and Technology, Beijing, China

*CORRESPONDENCE
Yingjie Li,
liyingjie820@126.com

SPECIALTY SECTION
This article was submitted to Structural Geology and Tectonics, a section of the journal Frontiers in Earth Science

RECEIVED 15 December 2022
ACCEPTED 20 March 2023
PUBLISHED 05 April 2023

CITATION
Wang S, Li Y, Jin S, Dong P, Zhang X, Zhao D, Kong X and Liu P (2023), Petrogenesis and tectonic implications of the Late Jurassic A-type granite in central Inner Mongolia, North China. *Front. Earth Sci.* 11:1124860. doi: 10.3389/feart.2023.1124860

Petrogenesis and tectonic implications of the Late Jurassic A-type granite in central Inner Mongolia, North China

Shuai Wang[1], Yingjie Li[2,3]*, Song Jin[4], Peipei Dong[2], Xiawei Zhang[1], Dongfang Zhao[2,4], Xingrui Kong[2] and Pengyu Liu[5]

[1]School of Earth Sciences and Resources, China University of Geosciences, Beijing, China, [2]College of Earth Sciences, Hebei GEO University, Shijiazhuang, China, [3]Hebei Key Laboratory of Strategic Critical Mineral Resources, Hebei GEO University, Shijiazhuang, China, [4]Geological Institute of China Chemical Geology and Mine Bureau, Beijing, China, [5]School of Science, China University of Geosciences, Beijing, China

Lying along the south of Mongol–Okhotsk Suture Belt (MOSB) in Horqin Right Middle Banner of Inner Mongolia, the Chuhuertu granite is exposed in the Duerji tectonic melange. Based on systematic field geological characteristics, petrology, geochemistry, and zircon U-Pb chronology, we determined the petrogenesis of pluton and the tectonic setting, and provide evidence for the dominant factors of granite magmatism of the study area. LA-ICP-MS zircon U-Pb dating showed an age of 155.6 ± 1.6 Ma, indicating that the formation age of the Chuhuertu granite is Late Jurassic. The granite is geochemically characterized by high SiO_2 (73.04–76.01 wt.%) and alkali (Na_2O + K_2O = 7.81–9.50 wt.%) but low CaO (0.20–0.98 wt.%) and MgO (0.10–0.22 wt.%). The granite has obvious negative Eu anomaly (Eu = 0.30–0.75), relative enrichment of Rb, Th, U, K, and Ga, depletion of Ba, Sr, P, and Ti, as well as high 10000Ga/Al (2.52–2.90), and TFeO/MgO (5.76–14.90). The differentiation index (DI) of the samples is 92.05–96.36. The petrological, mineralogical, and geochemical characteristics of the granite show the characteristics of highly differentiated A-type granite. In accordance with the region, Mesozoic A-type granites have positive correlation $\varepsilon_{Nd}(t)$ values, which suggest that the granite may have formed through partial melting of intermediate basic crust in neoaccretion under low pressure and high temperature, and subsequent crystallization differentiation. Therefore, Chuhuertu granite is the product of extension of the closure of the Mongol–Okhotsk Ocean (MOO), and, together with other A-type granites distributed in mid-eastern Inner Mongolia, indicates extensive middle and lower crust extension in the Late Jurassic.

KEYWORDS

A-type granite, late Jurassic, post orogenic extension, Mongol–Okhotsk Ocean, Inner Mongolia

1 Introduction

The southeastern Central Asian Orogenic Belt (CAOB), which is distributed throughout central Inner Mongolia in North China, is a key area for understanding the tectonic evolution of the CAOB, the world's largest Phanerozoic accretionary orogen between the Siberian Craton (SC) to the north and the Tarim and North China Craton (NCC) to the

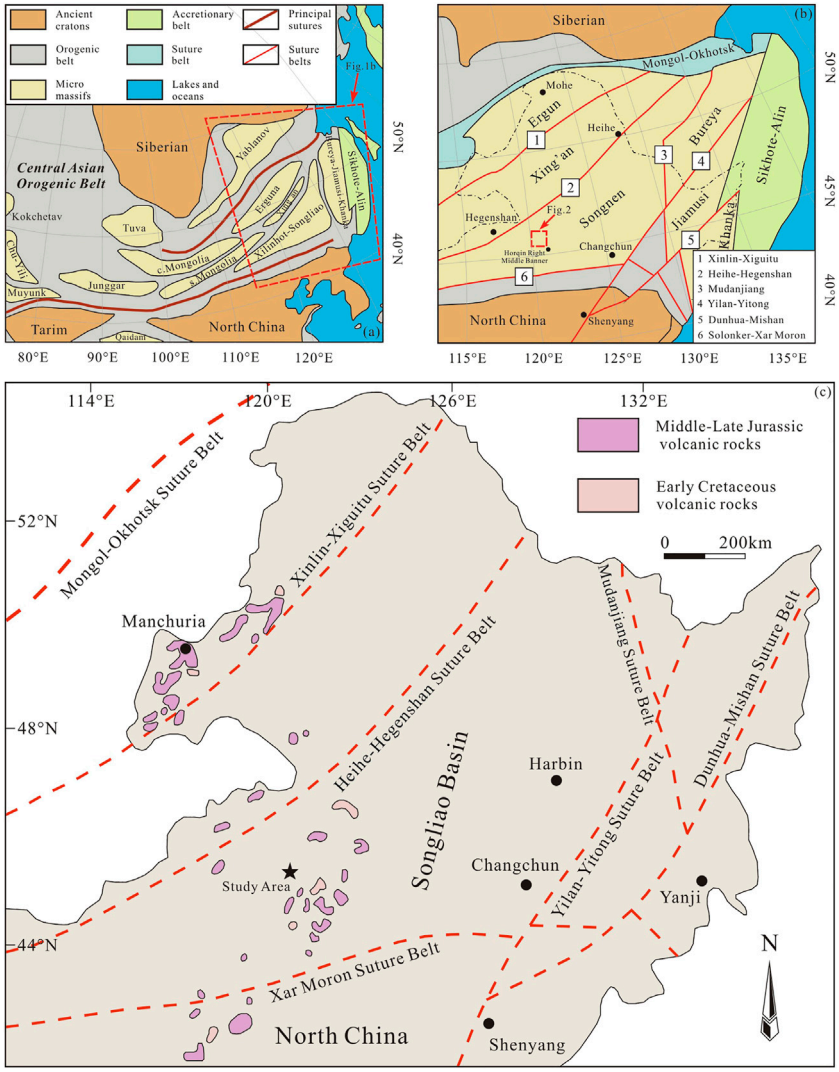

FIGURE 1
(A) Tectonic framework of the North China–Mongolia segment of the Central Asian Orogenic Belt (adapted from Liu et al., 2017). **(B)** Simplified geological map of NE China showing the main tectonic subdivisions (adapted from Zhou et al., 2015a). **(C)** Distribution map (adapted from Xu et al., 2013) of Middle-Late Jurassic and Early Cretaceous volcanic rocks in NE China.

south (Figure 1A) (Xiao et al., 2003; Windley et al., 2007). It is characterized by a series of island arcs, forearc and back-arc basins, ophiolitic belts, and microcontinental fragments with ages ranging from the Neoproterozoic to the Mesozoic (Jahn et al., 2000; Zhang et al., 2009a; Zhang et al., 2014; Li et al., 2018; Cheng et al., 2014; Cheng et al., 2020; Li et al., 2020; Liu et al., 2021). Before the Early Mesozoic, the southeastern CAOB was strongly influenced by the Paleo-Asian Ocean (PAO) tectonic regime (Nozaka and Liu, 2002; Liu et al., 2005; Miao et al., 2008; Jian et al., 2010; Safonova et al., 2017). There are two main viewpoints on the final closure time of the PAO. One viewpoint is based on the chronology and geochemistry of ophiolites and Carboniferous–Permian intrusive rocks. It is believed that the PAO continued to subduct from the Ordovician to the Permian, until the closure during the Late Permian–Early Triassic (Xiao et al., 2003; Jian et al., 2010; Li et al., 2018; Li et al., 2020). The other viewpoint is based on the study of orogenic belt structure, tectonic deformation, stratigraphic unconformity, and post orogenic A-type granite, and suggests that the PAO was closed before the Late Devonian–Early Carboniferous (Xu et al., 2014; Shao et al., 2015). During the Jurassic, with the final closure of the PAO, the southeastern CAOB was already in the tectonic environment of the Paleo-Pacific Ocean (PPO) and MOO tectonic regimes (Meng et al., 2011; Xu et al., 2013; Wang et al., 2015; Wu et al., 2017; Gao et al., 2021; Jiang et al., 2021). Thus, it is considered an ideal region in which to study the PAO tectonic regime and the superposition of MOO and PPO tectonic regimes during the Late Jurassic period.

The multi-plate convergence in NE China has resulted in a widespread occurrence of voluminous Late Mesozoic granitic–magmatic rocks, making it one of the world's largest granitic provinces (Wu et al., 2011; Xu et al., 2013). However, researchers have yet to clarify the trigger system of Late

Mesozoic granitic magmatism, especially for Late Jurassic granitic magmatism.

According to some researchers, the Late Jurassic granitic magmatism in NE China has been connected to flat-slab subduction of the PPO plate (Zhang et al., 2010; Ji et al., 2019). Several additional studies hypothesized that the MOO slab retreat and oceanic ridge subduction (Deng et al., 2019), as well as orogenic collapse following the closure of the MOO, were responsible for the Late Jurassic granitic magmatism in NE China (Xue et al., 2015; Li et al., 2018). These Late Jurassic granitic magmatic rocks in NE China are mainly located in the Ergun-Xing'an Massifs, southwestern Songnen Massif, and at the northern margin of NCC. The perspectives described previously are almost entirely based on the Jurassic tectonic magmatism in the Ergun, southwestern Songnen, and the northern Xing'an Massifs. However, the southeastern CAOB west of the Greater Xing'an Range has received little attention (Gillespie et al., 2017). As a result, additional research on the Late Jurassic igneous rocks in the southeastern CAOB is required to constrain its Jurassic tectonic setting.

In general, granitic rock types with various origins have a remarkable correlation with the tectonic environment (Pearce, 1996). Hence granitoids may provide important information regarding the coeval tectonic setting. A Late Jurassic granite was identified during our investigation in the southeastern CAOB and classed as an A-type granite. These findings, combined with the existing geochronology and geochemistry results for Jurassic-Early Cretaceous magmatic rocks in the southeastern CAOB (Zorin, 1999; Parfenov et al., 2001; Wang et al., 2006; Xu et al., 2013; Jiang et al., 2021), provide petrological, geochemical, and chronological evidence for determining the dominant factors controlling the Late Jurassic granite magmatism in the region.

2 Geological setting

The southeastern CAOB is bordered by the Pacific tectonic system to the east, the northern margin of NCC to the south, and the southern margin of SC to the north (Figure 1A), and formed by collision and suture of several microcontinental fragments (Liu et al., 2017). From north to south, it is divided into Ergun Massif, Xing'an Massif, Songnen Massif, and Bureya–Jiamusi–Khanka Massif by Xinlin–Xiguitu Suture Belt, Heihe–Hegenshan Suture Belt, and Mudanjiang Suture Belt (Figure 1B).

The southeastern CAOB is characterized by large-scale Phanerozoic magmatism (Wu et al., 2002; Wu et al., 2011). The Paleozoic magmatism in the southeastern CAOB is considered the result of southward subduction of the PAO plate (Zhang et al., 2009b). The Late Triassic tectonomagmatic events may have been related to the slab retreat of the subducting MOO (Meng et al., 2020). During the Jurassic and Cretaceous, the southeastern CAOB experienced overprinting effects from the Paleo-Pacific tectonic regime in the east (Wu et al., 2002; Wu et al., 2011; Zhu and Xu, 2019) and the Mongol–Okhotsk tectonic regime in the north (Wang et al., 2015; Wang et al., 2017).

The subduction of the Paleo-Pacific plate beneath the Northeast Asian continental margin has been differentially considered to have occurred at the Early Permian, the Triassic, or the Jurassic (Wang et al., 2017). Recently, growing evidence indicates that the subduction of the Paleo-Pacific plate started no later than the Early Jurassic (Xu et al., 2013; Zhang et al., 2018; Ji et al., 2019; Gao et al., 2021). Furthermore, the previous study suggested that low-angle flat slab subduction of the Paleo-Pacific plate beneath the eastern Eurasia continent occurred during the Jurassic, and then, the subducting slab experienced a slab rollback during the Early Cretaceous (Ji et al., 2019). On the other hand, although the timing of the opening of the MOO remains controversial, its subduction history has been constrained to the period from the Devonian to the Jurassic (Donskaya et al., 2013). The MOO closed in a scissor-like pattern and finally formed the MOSB, which was related to the collision between the SC in the north and the Central Mongolian Massif in the south, from west to east (Donskaya et al., 2013). Thus, many researchers suggested that the western part of the MOO closed earlier, i.e., in the Early-Middle Jurassic (Parfenov et al., 2001; Zhang et al., 2020), whereas the eastern part closed later, i.e., in the Late Jurassic–Early Cretaceous (Donskaya et al., 2013).

Jurassic–Cretaceous granitoids developed mainly in NE China, but have been reported, albeit rarely, in southeastern Inner Mongolia. Furthermore, through zircon U-Pb dating of 370 samples from granites widely developed in NE China, and combining those data with 63 ages obtained by other researchers, Wu et al. (2011) concluded that Jurassic granites developed mainly in the east and Cretaceous granites in the west. Jurassic granitoids in the east portion of NE China were likely related to the subduction of the Pacific plate, whereas the contemporaneous granitoids in the Erguna Massif in the northwest might be related to the subduction and subsequent closure of the MOO (Wu et al., 2011).

The newly discovered granite described here is located in the Chuhuertu farm area, ~40 km to the northwest of the Horqin Right Middle Banner. The Chuhuertu granite is exposed in the southwest of the Duerji tectonic melange. The pluton is distributed as a small stock in the ENE-WSW, of about 3.5 km length and 1 km width, with an exposed area of about 3.5 km^2. The southeast intrudes Late Triassic syenogranite, the northwest is intruded by Early Cretaceous monzonitic granite, and the pluton is partially intruded by Early Cretaceous granite-porphyry and covered by Quaternary rocks. The main rock type is syenogranite, the middle is medium-grained syenogranite, and the edge is transited to fine-grained, without obvious mylonitization (Figure 2). The Duerji tectonic melange is composed of "matrix" and "blocks." The "matrix" is mainly a set of marine clastic rocks with strong deformation and weak metamorphism, composed of tectonic schist, metasandstone, and phyllite, and some of them have the characteristics of flysch sedimentary formation, formed in the tectonic environment of an active continental margin. On the other hand, the "blocks" rock type is pyroxene amphibolite, amphibolite, basalt, diabase, and diorite, and has no significant deformation. The marine clastic rocks are strongly deformed. Due to strong compression, crumple developed and local fractures are sandwiched between magmatic rocks as fault gouges. The surface outcrops are mainly magmatic rocks, which are wrapped in marine clastic rocks as irregular blocks. Different magmatic rocks are also in fault contact, and the edges are developed with different degrees of schistosity. Simultaneous schistosity or mylonitic foliation is developed at the contact segment of rock faults (Jin, 2020).

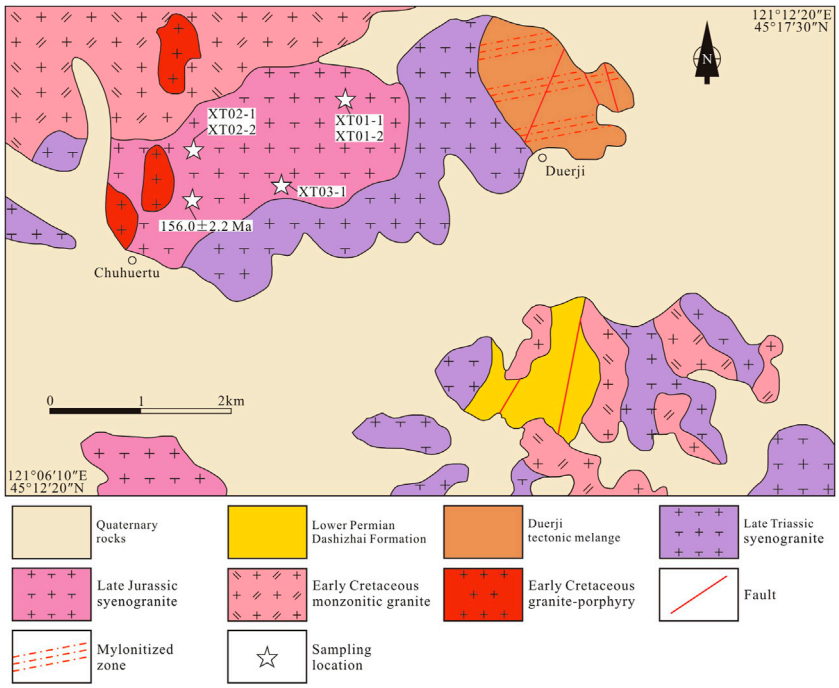

FIGURE 2
Simplified geological map of the Chuhuertu region in Horqin Right Middle Banner, Inner Mongolia.

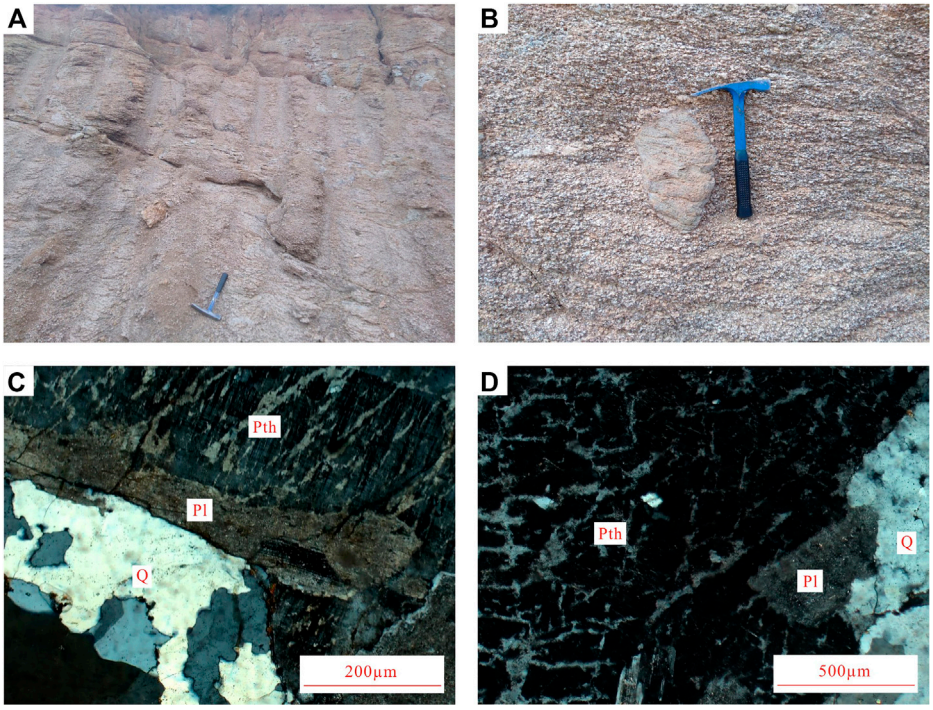

FIGURE 3
Macrofeatures and photomicrographs of the granite in Chuhuertu. **(A)** Macrofeatures; **(B)** field occurrence; **(C,D)** micrographs of the granite. Pl, plagioclase; Pth, perthite; Q, quartz.

10.3389/feart.2023.1124860

TABLE 1 Major and trace element data from Chuhuertu granite.

Sample	XT01-1	XT01-2	XT02-1	XT02-2	XT03-1	A-type granite worldwide	A-type granite in China
Major element (wt%)[a]							
SiO_2	74.30	74.89	75.28	76.01	73.04	73.81	73.55
TiO_2	0.17	0.19	0.18	0.11	0.15	0.26	0.23
Al_2O_3	13.02	13.01	12.50	12.15	13.85	12.40	12.81
FeO^{Tb}	1.66	1.21	1.46	1.49	1.36	2.70	2.46
MnO	0.04	0.06	0.06	0.04	0.05	0.060	0.090
MgO	0.20	0.21	0.22	0.10	0.15	0.20	0.27
CaO	0.54	0.98	0.31	0.20	0.35	0.75	0.82
Na_2O	3.42	3.56	3.99	3.58	4.69	4.07	3.76
K_2O	4.73	4.25	5.44	5.11	4.81	4.65	4.69
P_2O_5	0.06	0.06	0.03	0.03	0.03	0.040	0.070
Total[c]	99.10	99.08	100.38	99.67	99.09		
LOI	0.87	0.63	0.82	0.78	0.55		
$K_2O + Na_2O$	8.15	7.81	9.43	8.69	9.50		
A/CNK	1.11	1.06	0.96	1.03	1.02		
A/NK	1.21	1.24	1.00	1.06	1.07		
TFeO/MgO	8.30	5.76	6.64	14.90	9.07		
DI	93.19	92.05	96.69	96.36	95.70		
Trace element (ppm)							
Rb	201	163	215	210	158	169	269.69
Zr	144	125	111	122	198	528	333.77
Hf	5.72	5.36	4.06	5.78	7.53		
Ta	1.39	1.20	0.82	0.75	1.30		
Sr	118	242	69.3	59.1	179	48	57.54
Sample	XT01-1	XT01-2	XT02-1	XT02-2	XT03-1	A-type granite worldwide	A-type granite in China
Ba	359	432	453	269	528	352	235.96
Nb	10.0	7.67	8.05	5.95	8.71	37	34.93
Ga	18.4	19.9	16.7	18.7	19.5	24.6	18.54
Th	26.3	18.0	27.9	21.3	27.8	23	
U	4.45	2.20	2.42	1.65	3.61	5.00	
La	32.6	30.1	15.8	30.8	28.4		
Ce	69.8	39.8	57.0	64.5	58.3		
Pr	7.91	7.30	4.45	7.00	6.4		
Nd	29.4	27.6	16.3	26.3	24.4		
Sm	5.80	4.50	3.36	4.80	4.40		
Eu	0.65	0.90	0.75	0.40	0.60		
Gd	4.52	3.50	2.75	4.10	4.00		
Tb	0.81	0.50	0.48	0.70	0.70		

(Continued on following page)

TABLE 1 (*Continued*) Major and trace element data from Chuhuertu granite.

Sample	XT01-1	XT01-2	XT02-1	XT02-2	XT03-1	A-type granite worldwide	A-type granite in China
Dy	4.99	2.70	3.13	4.00	4.20		
Ho	1.01	0.50	0.62	0.80	0.90		
Er	2.92	1.60	1.79	2.40	2.50		
Tm	0.48	0.30	0.33	0.40	0.40		
Yb	3.30	2.10	2.26	2.90	2.80		
Lu	0.54	0.40	0.33	0.40	0.50		
Y	28.6	15.5	17.8	21.9	24.3	75	54.03
Total REE	164.73	121.76	109.35	149.55	138.38		
LREE	146.16	110.18	97.66	133.83	122.49		
HREE	18.57	11.58	11.69	15.72	15.89		
LREE/HREE	7.87	9.51	8.35	8.51	7.71		
$(La/Yb)_N$	7.09	10.14	5.01	7.57	7.17		
δEu	0.39	0.68	0.75	0.30	0.43		
10,000*Ga/Al	2.67	2.88	2.52	2.90	2.66	3.75	
T_{Zr} (°C)	787	771	750	767	803		

[a]All oxide contents of the samples have been recalculated to 100% on a volatile-free basis.
[b]FeO^T as total FeO.
[c]Total before normalization.
Data sources: A-type granite worldwide and in China (Wu et al., 2007).

3 Samples and analytical methods

3.1 Samples

The Chuhuertu granite is generally grayish white to pink in color, with medium-fine-grained hypidiomorphic granular structure and stripe structure, and massive texture (Figures 3A, B). This rock contains mainly alkali feldspar (55–60 vol.%), quartz (−20 vol.%), plagioclase (10–15 vol.%), biotite (−5 vol.%), and accessory magnetite. Mineral particle size is generally 0.2–5 mm. The alkaline feldspar is in the form of hypidiomorphic–xenomorphic plate-type, mainly composed of orthoclase, perthite, and microcline feldspar, with a particle size of 0.2–5 mm. Among them, perthite is primarily in the form of fine veins and branches arranged in the same direction (Figure 3D). The plagioclase is mainly andesine and oligoclase, in the form of euhedral-hypidiomorphic plate-type, with polysynthetic twin, occasionally with ring structure, and a particle size of 0.2–4 mm. Quartz is found as fill between plagioclase and alkali feldspar, with xenomorphic granular texture, a particle size of 0.2–5 mm, cracks, and wavy extinction. Biotite is distributed in a scale-blade shape with a diameter of 0.2–2 mm (Figures 3C, D).

In order to study the geochemical and chronological characteristics of the Chuhuertu granite, five geochemical samples were collected (Table 1), along with one (Table 2) zircon U-Pb sample, from different parts of the pluton on the basis of detailed field geological observations. The weathering degree of the samples was low, and free from oxidation, pollution, and obvious alteration. See Figure 2 for the sampling locations.

3.2 Analytical methods

The whole-rock geochemical analyses were undertaken at the Central Laboratory of China Chemical Geology and Mine Bureau, Beijing, China. The zircon selection and target making were completed by the Beijing Kehui Testing Technology Co., Ltd., Beijing, China, and zircon U-Pb isotopic analyses were undertaken at the Beijing SHRIMP Center.

A Zsx Primus II wavelength dispersive X-ray fluorescence spectrometer (XRF) produced by RIGAKU, Japan, was used for the analysis of major elements in the whole rock; the X-ray tube was a 4.0 Kw end window Rh target. All major element analysis lines were kα, and the standard curve used the national standard material: the rock standard sample GBW07101-14. The relative standard deviation (RSD) was less than 2%.

Trace-element analyses of whole-rock were conducted on an Agilent 7700e ICP-MS. The detailed sample-digesting procedure was as follows: 1) Sample powder (200 mesh) was placed in an oven at 105°C for drying for 12 h; 2) an amount of 50 mg of sample powder was accurately weighed and placed in a Teflon bomb; 3) a measure of 1 mL of HNO_3 and 1 mL of HF were slowly added into the Teflon bomb; 4) the Teflon bomb was enclosed in a stainless steel pressure jacket and heated to 190°C in an oven for >24 h; 5) after cooling, the Teflon bomb was opened and placed on a hotplate at 140°C and evaporated to incipient dryness, and then, 1 mL HNO_3 was added and evaporated to dryness again; 6) a measure of 1 mL of HNO_3, 1 mL of MQ water, and 1 mL of internal standard solution at 1 ppm were added, and the Teflon bomb was resealed and placed in the oven at 190°C for >12 h; 7) the final solution was transferred to a

TABLE 2 LA-ICP-MS zircon U-Pb isotopic analysis of the Chuhuertu granite.

Spot no.	Element (ppm)		Th/U	Isotopic ratios						Apparent age (Ma)					
	Th	U		$^{206}Pb/^{238}U$	1σ	$^{207}Pb/^{235}U$	1σ	$^{207}Pb/^{206}Pb$	1σ	$^{206}Pb/^{238}U$	1σ	$^{207}Pb/^{235}U$	1σ	$^{207}Pb/^{206}Pb$	1σ
TW04 Chuhuertu granite															
01	195	470	0.42	0.0238	0.0003	0.1628	0.0050	0.0496	0.0014	152	2	153	4	176	65
02	200	486	0.41	0.0243	0.0004	0.1648	0.0050	0.0492	0.0014	155	2	155	4	167	73
03	106	228	0.46	0.0247	0.0005	0.1695	0.0083	0.0497	0.0022	157	3	159	7	183	104
04	111	218	0.51	0.0248	0.0003	0.1798	0.0082	0.0529	0.0025	158	2	168	7	324	109
05	395	682	0.58	0.0247	0.0002	0.1726	0.0046	0.0507	0.0014	157	2	162	4	228	68
06	100	247	0.41	0.0248	0.0004	0.1756	0.0083	0.0513	0.0024	158	2	164	7	254	110
07	415	882	0.47	0.0243	0.0002	0.1812	0.0047	0.0540	0.0013	155	1	169	4	372	56
08	92	152	0.60	0.0242	0.0007	0.1807	0.0125	0.0543	0.0037	154	5	169	11	383	156
09	130	299	0.44	0.0248	0.0003	0.1630	0.0083	0.0482	0.0027	158	2	153	7	109	130
10	418	882	0.47	0.0244	0.0003	0.1791	0.0063	0.0533	0.0018	155	2	167	5	343	78

10.3389/feart.2023.1124860

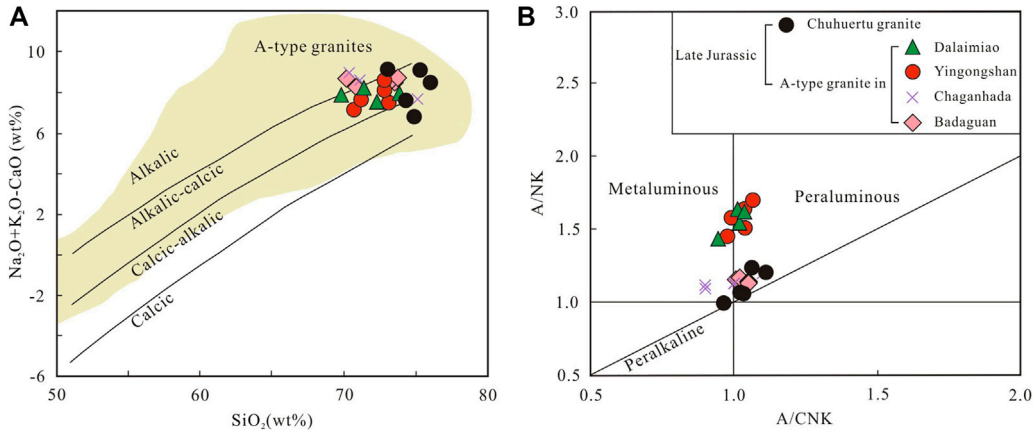

FIGURE 4
(A) SiO_2 versus Na_2O + K_2O—CaO diagram (adapted from Frost and Frost, 2008) and **(B)** A/CNK versus A/NK diagram (adapted from Maniar and Piccoli, 1989) for the granite in Chuhuertu. Data sources: A-type granite in Dalaimiao (Xue et al., 2015), Yingongshan (Gao et al., 2021), Chaganhada (Gao et al., 2022), and Badaguan (Tang et al., 2015).

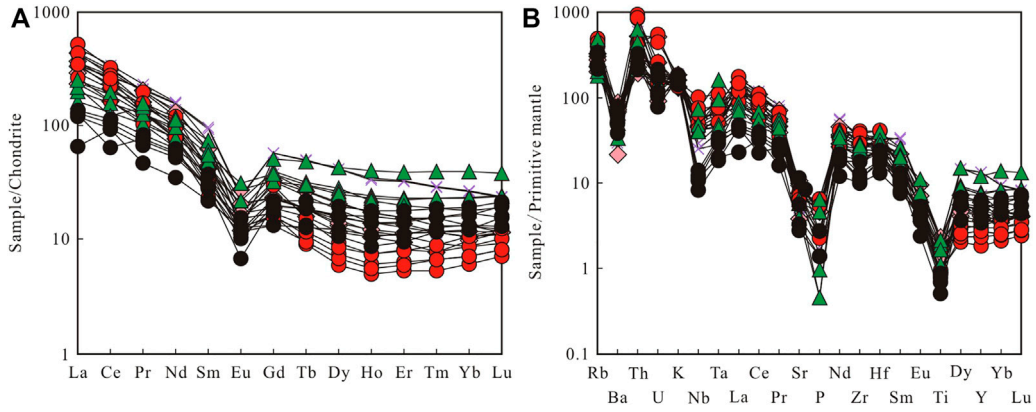

FIGURE 5
(A) Chondrite-normalized REE diagram and **(B)** primitive-mantle-normalized trace element diagram for the granite in Chuhuertu. The normalizing values are from Sun and McDonough (1989). Symbols are the same as in Figure 4.

polyethylene bottle and diluted to 100 g *via* the addition of 2% HNO_3.

The zircon U-Pb dating method used was LA-ICP-MS *in-situ* U-Pb isotope dating, and the test instrumentation included a NWR193 laser ablation system and Jena PQMS inductively coupled plasma mass spectrometry. The depth of laser denuded zircons was 20–40 μm. The diameter of the denudation beam spot was 35 μm. The international standard zircon 91,500 was used as the external zircon age standard for isotopic fractionation correction, and the element content was corrected with the standard sample NIST SRM610 as the external standard and ^{29}Si as the internal standard. The test results were processed and mapped using ICPMSDataCal software (Liu et al., 2008), and the ^{208}Pb correction method was used to correct the common lead (Anderson, 2002).

4 Analytical results

4.1 Major and trace element geochemistry

The Chuhuertu granite has LOI content ranging from 0.55 to 0.87 wt.% (Table 1), consistent with petrographic evidence for partial alteration. In addition, the elements Li, Rb, Cs, K, U, and P may be readily mobilized in rocks during hydrothermal alteration (Hart et al., 1999; Bach et al., 2001). Consequently, in the following descriptions and discussion, the major element contents were normalized to 100 wt.% on an anhydrous basis, considering all Fe as FeO; we preferentially used elements that are relatively insensitive to alteration, such as SiO_2, Al_2O_3, TiO_2, MgO, Fe_2O_3, high-field-strength elements (HFSE), rare-earth elements (REE), Th, and Ba.

Chemical data for five whole-rock samples of the Chuhuertu granite are presented in Table 1. The samples showed high SiO_2

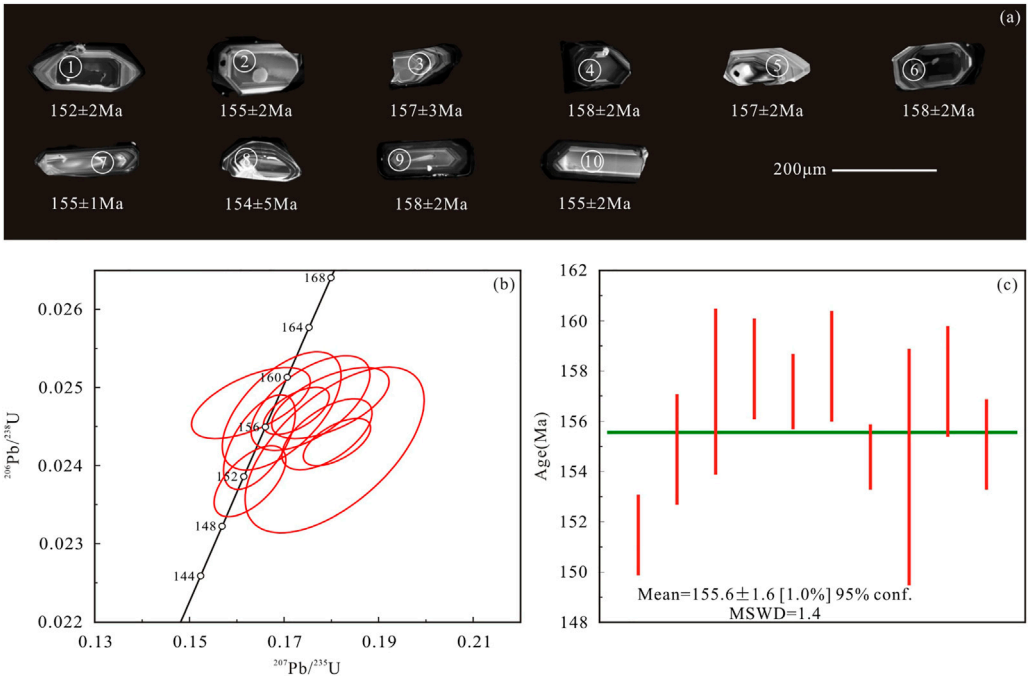

FIGURE 6
(A) Representative cathodoluminescence (CL) images, **(B)** concordia curves, and **(C)** weighted mean age of LA-ICP-MS U-Pb data for the granite in Chuhuertu.

(73.04–76.01 wt.%) and K_2O (4.25–5.44 wt.%) content. At the same time, the samples had high Na_2O (3.42–4.69 wt.%) content, and the high total K_2O + Na_2O content (7.81–9.50 wt.%) suggested material rich in alkali. The SiO_2 versus Na_2O + K_2O – CaO diagram (Figure 4A) indicates samples with calcic-alkali to alkali features. The samples had low CaO (0.20–0.98 wt.%), MgO (0.10–0.22 wt.%), P_2O_5 (0.03–0.06 wt.%), and TiO_2 (0.11–0.19 wt.%) content. The Al_2O_3 content of samples was high, at 12.86–13.45 wt.%. In the A/CNK versus A/NK diagram (Figure 4B), samples fall into quasi-aluminous and peraluminous areas, with A/CNK values (molar $Al_2O_3/(CaO + Na_2O + K_2O)$ = 0.96–1.11) and A/NK values (molar $Al_2O_3/(Na_2O + K_2O)$ = 1.00–1.24) showing weakly peraluminous characteristics.

The total amount of rare earth elements (ΣREE) found in the samples was in the range of 109.35–164.73 ppm, with an average of 136.75 ppm (Table 1). The normalized REE distribution diagram of chondrites indicates "Seagull type" (Figure 5A), with obvious negative Eu anomaly, and δEu of 0.30–0.75, with an average value of 0.51. The REE curve for the samples has a generally gentle right dip, the light REE (LREE) appears slightly enriched, and the heavy REE (HREE) curve is relatively flat. The negative Eu of the samples is abnormally significant, suggesting that the pluton may be affected by the fractional crystallization of plagioclase or related to residual plagioclase in the source area (Eby, 1992). In terms of trace elements, the samples were enriched in Rb, Th, U, K, and Ga, and depleted in Ba, Sr, P, and Ti (Figure 5B), showing the unique component characteristics of A-type granite (Eby, 1992).

4.2 Zircon U-Pb ages

The representative zircon U-Pb data are listed in Table 2. Most zircon grains separated from the granite sample TW04 showed similar crystal shapes and subhedral to euhedral morphologies, with no evidence of resorption or inherited cores. The zircon grains were transparent, colorless, and showed oscillatory zoning, consistent with a magmatic origin (Figure 6A). All zircon grains had high Th/U ratios (0.41–0.60); Table 2), supporting a magmatic origin (Hoskin and Schaltegger, 2003). Ten analyses of zircons from sample TW04 yielded concordant zircon $^{206}Pb/^{238}U$ ages, ranging from 152 ± 2 to 158 ± 2 Ma. These data yielded a weighted-mean age of 155.6 ± 1.6 Ma (MSWD = 1.4) (Figures 6B, C), interpreted as the crystallization age of the Chuhuertu granite.

5 Discussion

5.1 Petrogenesis of the Chuhuertu granite

The Chuhuertu granite was characterized by high concentrations of SiO_2 and K_2O + Na_2O, but low CaO, MgO, P_2O_5, and TiO_2, with obvious negative Eu anomaly. The trace elements Rb, Th, K, Ta, and Hf were relatively enriched, while the elements Ba, Sr, P, and Ti were relatively depleted, and all had high (Na_2O + K_2O)/CaO (15.08–21.39) and TFeO/MgO (29.16–57.82) values. At the same time, the Chuhuertu granite had high Ga (16.70–19.86 ppm) values, and its 10000Ga/Al value was 2.52–2.90. Except for sample XT02-1, the samples had greater

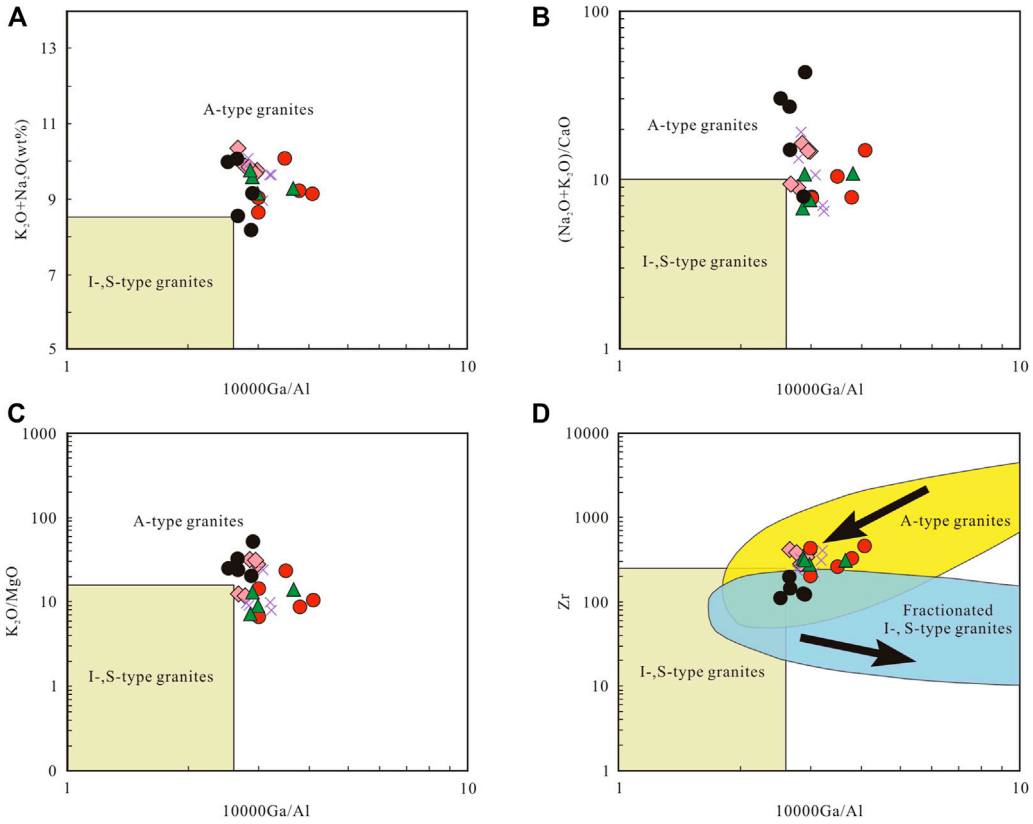

FIGURE 7
10000Ga/Al versus $K_2O + Na_2O$ **(A)**, $(N_2O + ka_2O)/CaO$ **(B)**, K_2O/MgO **(C)**, and TFeO/MgO **(D)** diagram (adapted from Whalen et al., 1987; Wu et al., 2017) for the granite in Chuhuertu. Symbols are the same as in Figure 4.

than the lower limit of 2.6 for A-type granite. In the four widely used 10000Ga/Al versus $K_2O + Na_2O$, $(N_2O + ka_2O)/CaO$, K_2O/MgO, and Zr granite discrimination diagrams (Figure 7), except for sample XT02-1 in Figure 7D, the samples fall into the A-type granite area. The aforementioned geochemical characteristics show that the Chuhuertu granite has the characteristics of A-type granite. However, the DI of the samples was found to be 92.05–96.36, and some samples plot in the fractional granite field (Figure 7D), which may be a result of crystallization fractionation. Crystallization fractionation could easily modify the geochemical composition of granite, and most of the highly fractionated granites have pseudo A-type features. Therefore, it remains unclear whether crystallization fractionation has taken place in Chuhuertu granite.

It is not a straightforward task to distinguish the highly fractionated from A-type granites, especially aluminous A-type granites. Whalen et al. (1987) found that A-type granites are low in Al but high in Ga and Zr concentrations, and then proposed that 10000Ga/Al = 2.6 and Zr = 250 ppm might indicate boundaries between A-type and other types of granites (A-type granite has 10000Ga/Al ratio > 2.6 and Zr > 250 ppm). However, quite a few highly fractionated granites also have a high 10000Ga/Al ratio similar to A-type granites (Perez-Soba and Villaseca, 2010; Breiter et al., 2013). Likewise, A-type granite, if intensively fractionated, is geochemically overlapping with highly fractionated granite (King et al., 2001). To address this problem, we adopted the classification method proposed by Wu et al. (2017). First, A-type granite is characterized by its high temperature of magma. However, the crystallization temperature of magma tends to decrease in the process of magmatic differentiation. Second, fractional crystallization will shift rock type from A-type to highly fractionated granite, as shown in Figure 7D. On the contrary, the fractionation of I- or S-type granites by crystal differentiation would increase their 10000Ga/Al ratios, and thus, another kind of evolutionary trend is observed (Figure 7D). Therefore, A-type granite can be effectively distinguished from highly fractionated I- or S-type granites, although the former occasionally shows an intensive magmatic differentiation. The data from samples from the Chuhuertu granite clearly showed an A-type granite differentiation trend (Figure 7D), indicating its A-type affinity. In addition, highly fractionated granitic magma is easily contaminated by country rocks due to its relatively prolonged crystallization time (Wu et al., 2017). During the early stage, the surrounding rocks are continuously assimilated by the magma, but the fractional crystallization leads to the surrounding rock being rarely observed in this granite. However, as the temperature of the magma gradually decreases with differentiation, the residual melt is not able to digest the surrounding rocks as assimilation proceeds. At the same time, the residual melt is low in capacity for movement, resulting in abundant xenocrysts of the surrounding rocks in the final solidified granite. Although the Chuhuertu granite has

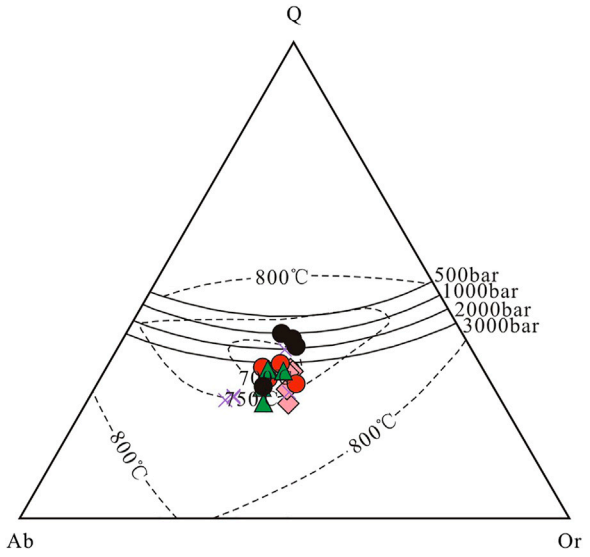

FIGURE 8
Q-Ab-Or-H_2O diagram (adapted from Chen et al., 2005) for the granite in Chuhuertu. Symbols are the same as in Figure 4.

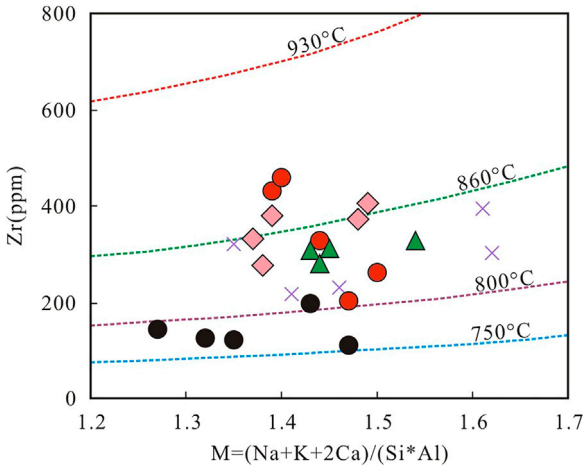

FIGURE 9
M values versus Zr content diagram (adapted from Gao et al., 2021) for the granite in Chuhuertu. Symbols are the same as in Figure 4.

undergone crystallization differentiation, there are few xenocrysts in the pluton. Therefore, the Chuhuertu granite may have been in the early stage of contamination when it crystallized. At the same time, in the A/CNK versus A/NK diagram (Figure 4B), the samples fall into quasi-aluminous and peraluminous areas, with A/CNK values (0.96–1.11) and A/NK values (1.00–1.24), indicating that the A-type granite should be weakly peraluminous, which is consistent with the geochemical characteristics of A-type granite in the eastern segment of CAOB (Liu et al., 2005; Zhou et al., 2010; Zhang et al., 2012; Shi et al., 2014; Xue et al., 2015).

A-type granites can be formed in a variety of petrogenetic processes, which can be summarized into the following three types: mixing of crust-derived acidic magma and mantle-derived basic magma (Griffin et al., 2002; Barbarin, 2005); low degree partial melting or crystallization differentiation of mantle-derived basaltic magma (Turner et al., 1992; Lee and Bachmann, 2014); and partial melting of crust-derived materials (Chappell and White, 2001; Sisson et al., 2005). The Chuhuertu granite has high SiO_2 content and narrow range. There are no contemporaneous mafic rocks or mafic enclaves, and Chuhuertu granite does not have the characteristics of crystallization fractionation of mantle-derived alkaline basaltic magma and mixing of mantle-derived magma and crust-derived magma formed by deep melting. The lower REE content and right-dipping REE diagram (Figure 5A) of the Chuhuertu granite indicate that there is no residual garnet in the source area. The strong depletion of Sr and Ba indicates that the residual phase in the source area contains feldspar, and the strong depletion of Sr and Eu (Figure 5B) reveals that the plagioclase in the source area is the main residual phase, reflecting that the source area is a shallow low pressure area (<10 kbar) without garnet residue and enriched plagioclase (Rapp and Watson, 1995), which should be the petrogenesis of partial high-temperature melting of intermediate basic crust in neoaccretion under low pressure and subsequent crystallization differentiation. These characteristics of Chuhuertu granite reveal that the area is in an extensional environment, similar to the petrogenesis of the A-type granite in the eastern segment of CAOB in mid-eastern Inner Mongolia (Zhang et al., 2012).

As for the high temperature anomaly required by the low pressure and high temperature melting of the shallow intermediate basic crust in neoaccretion, more and more scholars believe that it is related to the post orogenic mantle-derived basaltic magma underplating caused by the upwelling of mantle materials in the asthenosphere induced by the previous subducted slab breaking-off and gravity collapse (Jahn et al., 2000; Bonin, 2007; Wu et al., 2007; Zhang et al., 2012; Xue et al., 2015). In mid-eastern Inner Mongolia, Mesozoic aluminous A-type granites generally have a positive $\varepsilon_{Nd}(t)$ value, which suggests that the underplating of mantle-derived magma related to slab break-off in the post-orogenic stage plays an important role in the formation of Mesozoic aluminum A-type granitic magma in mid-eastern Inner Mongolia (Jahn et al., 2000; Chen et al., 2008; Zhou et al., 2010; Shi et al., 2014; Xue et al., 2015). In terms of petrography, perthite (Figures 3C, D) is found locally in the samples and inherited zircon is not found in S-type granite. This reveals that the melt was high-temperature and water poor, and that the early magmatic crystallization occurred under high-temperature conditions. These characteristics also reflect the petrogenesis of partial high-temperature melting of the intermediate basic crust in neoaccretion under low pressure and its subsequent differentiation.

5.2 Temperature and pressure conditions of the magmatic source

It is generally believed that A-type granite is formed under high temperature and low pressure, which generally occurs in the shallow middle and upper crust (Clemens et al., 1986). Therefore, the calculation of temperature and pressure conditions for the formation of Chuhuertu pluton indicates A-type granite from the

side. At the same time, the temperature and pressure conditions of magma formation can be used to speculate on the depth of its magmatic source, thus providing constraints for the origin and evolution mechanism of magma.

5.2.1 Q-Ab-Or-H_2O equilibrium pressure calculation

Based on many petrological experimental data, predecessors summarized the equilibrium phase diagram of quartz (Q), albite (Ab), orthoclase (Or), and H_2O, which can be used to calculate temperature and pressure during magma formation (Whitney and Stormer, 1985; Holland and Blundy, 1994; Rajesh, 2000; Liu et al., 2003; Chen et al., 2005).

Q, Ab, and Or are CIPW standard mineral content. It can be seen from the Q-Ab-Or-H_2O equilibrium phase diagram (Figure 8) of the granite that the formation pressure is about 0.1–0.3 Gpa, equivalent to the depth of 4–11 km, indicating shallow crust. However, the formation temperature is about 700°C–750°C, which is slightly lower than the average level of A-type granite (800°C–900°C). These results may be due to the disaggregation of fluid, which reduces the near solidus temperature of A-type granite, while the temperature value of the Q-Ab-Or-H_2O equilibrium phase diagram is the eutectic temperature (Liu et al., 2003). In addition, this may be caused by crystallization fractionation of Chuhuertu granite (Wu et al., 2017).

5.2.2 Zircon saturation thermometry

Compared with water-rich and low-temperature I- and S-type granites, A-type granites are generally considered to have been formed by relatively anhydrous and high-temperature magmas (Loiselle and Wones, 1979; Bonin, 2007). Zircon saturation thermometry (T_{Zr}) can provide a simple and robust means of estimating magma temperatures (Watson, 1979). Because zircon crystallizes early in acid magma, the zircon saturation temperature can be approximately regarded as the temperature of magma formation. This paper adopts the simulation formula of T_{Zr} (°C) = 12,900/[2.95 + 0.85M + lnD_{zr} (zircon/melt)]-273 zircon solubility-saturation temperature obtained by Watson (1979). Here, D is the distribution coefficient. Assuming that the whole rock Si + Al + Fe + Mg + Ca + Na + K + p = 1 (atomic fraction), the whole rock petrochemical parameter M = (2Ca + Na + K)/(Si × Al). When the whole-rock zircon minerals Zr and Hf are not corrected, Zr = 497,626 × 10^{-6} in pure zircon. At the same time, the Zr contents of the whole rock are approximately used to represent the Zr contents in the melt. The calculated sample formation temperature is basically concentrated between 750°C and 803°C (Figure 9), which is close to, but slightly lower than, the average temperature of A-type granite formation. It is also understood that the crystallization fractionation of the Chuhuertu granite reduces its crystallization temperature (Wu et al., 2017).

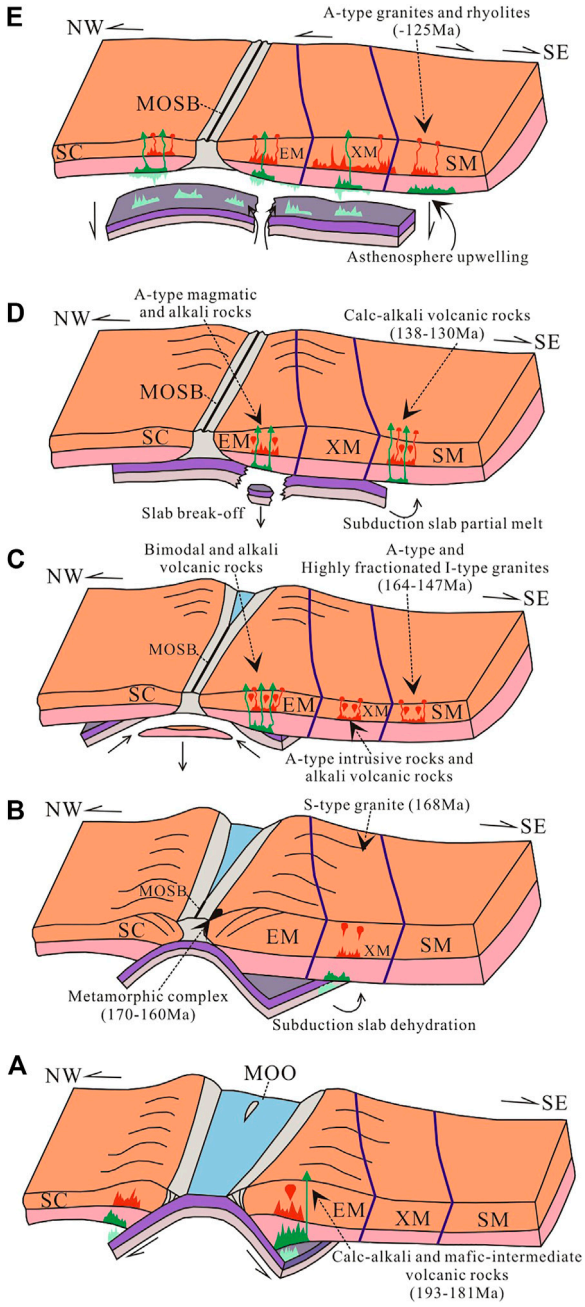

FIGURE 10
Schematic diagram (adapted from Zhang et al., 2020) showing a petrogenetic model for Late Mesozoic magmatic rocks in the southern Great Xing'an Range. SC, Siberian Craton; EM, Erguna Massif; XM, Xing'an Massif; SM, Songliao Massif; MOO, Mongol-Okhotsk Ocean; MOSB, Mongol-Okhotsk Suture Belt.

5.3 Tectonic implications of the granite in Chuhuertu: Under the control of the Mongol–Okhotsk or the Paleo-Pacific tectonic regime?

For a long time, the driving mechanism of the evolution of the Northeast Asian continent has been generally manifested in the subduction of the Paleo-Pacific plate and the closure of MOO (Meng et al., 2011; Xu et al., 2013; Wang et al., 2015; Wu et al., 2017).

Recently, Ji et al. (2019) reported a Late Jurassic oceanic crust-derived low-K adakitic lava in the Hailar Basin and linked it to the flat-slab subduction of the Paleo-Pacific plate. The low-K adakitic lava was considered to represent the final pulse of slab-melt-related volcanism, which also suggests that the Hailar Basin might be the farthest position ever reached by the subducting Paleo-Pacific plate

(Ji et al., 2019). When the flat-slab of the Paleo-Pacific plate subducted under the Hailar–Tamtsag Basin and the Greater Xing'an Range region with thick lithosphere, the increased subduction depth of the slab led to the eclogitization of the originally light oceanic crust, which increased the density of the subducted slab and returned it to negative buoyancy (Antonijevic et al., 2015). It was suggested that the flat-slab of the subducted slab was also unstable and decoupled from the overlying mantle wedge, which led to the rollback accompanied by the gravitational subsidence of the subducted slab (Antonijevic et al., 2015). The appearance of Late Jurassic A-type granites in the Hailar–Tamtsag Basin and the Greater Xing'an Range (Yang et al., 2014; Jiang et al., 2021) also suggests that the upwelling of asthenosphere mantle material caused by the slab rollback of the Paleo-Pacific plate in the Late Jurassic-Early Cretaceous provided some high-temperature conditions required for the formation of A-type granite magmas in the region (Ji et al., 2019).

In addition, many scholars believe that the destruction of NCC is related to the subduction of the Paleo-Pacific plate (Wu et al., 2005; Zhang et al., 2014; Zhu and Xu, 2019; Gao et al., 2021), and its remote effects caused large-scale Early Cretaceous massive magmatism and craton destruction of NCC, resulting in large-scale extension of the middle and lower crust (Zhang et al., 2009b; Zhang et al., 2014; Zhu and Xu, 2019; Gao et al., 2021). The lithospheric reconstruction of NCC by the Middle-Late Jurassic Paleo-Pacific plate was mainly limited to the eastern part of North China and the eastern part of Western Liaoning. A study of the lithofacies paleogeography showed that the Jurassic strata in the eastern part of NCC are obviously lost, which indicates that the area was in a tectonic setting of uplift in the Jurassic (Zhu and Xu, 2019), which was manifested by crustal thickening caused by subduction and compression, and formed a NE trending low-temperature and water-rich granite belt between the Jurassic granite in the eastern part of North China and the Zhangguangcai Ridge in NE China, which is parallel to the Paleo-Pacific subduction belt at the edge of Eurasia (Wu et al., 2005). The Chuhuertu granite is located in the Mesozoic magmatic active belt of the Greater Xing'an Range in the southeastern CAOB, and its emplacement age is Late Jurassic (ca. 156 Ma). Through petrology, mineralogy, and geochemistry, it is classified as A-type granite (water poor and formed under low pressure and high temperature). It is obvious that the Chuhuertu granite is unlikely to be the product of the subduction of the Paleo-Pacific plate in terms of space, time, and rock type.

The study area is located in southeastern Inner Mongolia-North Hebei. There are many Late Jurassic–Early Cretaceous volcanic eruption basins in the region. The crater is obviously distributed in the NE. The volcanic eruption basins are mainly depression type, and a large number of collapse calderas are developed inside. The long axis directions of the basins and the calderas are basically the same, both of which are in the NE, indicating that they are mainly controlled by large extension faults in the NE (Meng et al., 2011; Xu et al., 2013; Jiang et al., 2021). The direction is consistent with that of MOSB. At the same time, the volcanic rocks in the Late Jurassic and Early Cretaceous have similar distribution ranges, which are only distributed west of the Songnen Basin-North Hebei line (Figure 1C) (Wang et al., 2006; Zhang et al., 2008; Meng et al., 2011; Xu et al., 2011; Xu et al., 2013), and show more extensive features exposed to the west. These characteristics indicate that the Late Jurassic–Early Cretaceous volcanic rocks in the study area are remotely affected by the Mongol–Okhotsk tectonic system on the northwest side.

Chuhuertu A-type syenogranite is located in southeastern Inner Mongolia-North Hebei, and its emplacement age is Late Jurassic (ca. 156 Ma). Combined with a series of Late Jurassic A-type granites (Chen et al., 2008; Xie et al., 2012; Xue et al., 2015; Zhu et al., 2020) determined successively in the southeastern CAOB and NCC in recent years, the middle and lower crust in this area have been shown to have generally been in an extensional flow state in the Late Jurassic. In addition, alkaline-subalkaline volcanic rocks and rhyolites were widely exposed in the Greater Xing'an Range and the North Hebei-Western Liaoning during the Late Jurassic and Early Cretaceous (Meng et al., 2011; Li, 2012; Peng et al., 2012; Wang et al., 2013). The alkaline volcanic rock associations of the two periods of volcanic rocks indicate the regional extensional environment, which correspond to the extensional environment after A and B phases of Yanshan movement, respectively, suggesting that the two periods of magmatic events are related to the evolution of the Mongol–Okhotsk tectonic system (Zheng et al., 2000). Therefore, based on spatial fit and temporal correlation, Late Jurassic magmatism in the southeastern CAOB was mainly controlled by the Mongol–Okhotsk tectonic regime. During the Early Jurassic, the southern subduction of the Mongol-Okhotsk oceanic plate resulted in the formation of calc-alkali and mafic-intermediate volcanic rocks in the Ergun region (Figure 10A) (Xu et al., 2013). During the Middle Jurassic, the closure of the western MOO was completed, and a continental collision resulted in crustal thickening. The partial melting of the thickened crust formed S-type granite on the Xing'an Massif (Figure 10B) (Li et al., 2018a). During the Late Jurassic, with the "scissors" closure of the MOO from west to east, the subduction zone retreated in the NE trending, resulting in the subsequent rollback of the subduction slab, causing the collapse and delamination of the thickened crust, triggering the asthenospheric mantle upwelling, leading to the extension of the continental lithosphere (Tang et al., 2015; Zhang et al., 2018). The Chuhuertu A-type syenogranite in the study area is the product of the orogenic extension setting after the closure of MOO, and its emplacement under a certain extension event (Figure 10C). In the early Early Cretaceous, the rapid closure of the eastern MOO provided high-speed subduction, pushing the slab forward and causing flat-slab subduction of the oceanic plate. As the subduction slab continued to advance southward and the mantle wedge retreated, a set of basic to intermediate-acidic arc volcanic rocks were formed by partial melting of the mantle wedge in the Greater Xing'an Range (Figure 10D) (Meng et al., 2011; Xu et al., 2013). In the late Early Cretaceous, after the ocean closed, the convergence power of the subduction slab disappeared, and the subduction oceanic crust gradually collapsed from south to north due to the influence of gravitational potential energy, resulting in crustal thinning, mantle upwelling, and partial melting of crustal

materials. A-type granite and rhyolite were formed in the Bahrain Left Banner-Zarut Banner in the southern segment of the Greater Xing'an Range (Figure 10E) (Zhang et al., 2020).

6 Conclusions

(1) Chuhuertu granite is exposed in the northwest of the Duerji tectonic melange in Horqin Right Middle Banner. The zircon U-Pb age of LA-ICP-MS is 155.6 ± 1.6 Ma, revealing that its emplacement age is Late Jurassic.

(2) The geochemical characteristics of Chuhuertu granite are high SiO_2 and alkali; low CaO and MgO; A/CNK = 0.96–1.11; A/NK = 1.00–1.24; obvious negative Eu anomaly; enrichment of Rb, Th, U, K, and Ga elements; relative loss of Ba, Sr, P, and Ti elements; and high values of 10000Ga/Al, TFeO/MgO, and DI. The geochemical characteristics indicate that it is highly differentiated A-type granite.

(3) Under conditions of low pressure and high temperature, the partial melting of basic–intermediate crust in neoaccretion and subsequent crystallization differentiation may represent the petrogenesis of Chuhuertu granite, while superimposing the influence of the Paleo-Pacific plate rollback. Chuhuertu granite is the product of extension of the closure of MOO and, together with other A-type granites distributed in mid-eastern Inner Mongolia, it indicates extensive middle and lower crust extension in the Late Jurassic.

Data availability statement

The original contributions presented in the study are included in the article/Supplementary Material, further inquiries can be directed to the corresponding author.

Author contributions

Conceptualization, YL; data curation, DZ and XK; formal analysis, PD and PL; investigation, SJ and XZ; writing—original draft, SW. All authors have read and agreed to the published version of the manuscript.

Funding

This research was funded by the National Natural Science Foundation of China (41972061), the China Geological Survey (1212011120711 and DD20160048-14), and the Science and Technology Innovation Team Program of Hebei GEO University (KJCXTD-2021-07).

Conflict of interest

The authors declare that the research was conducted in the absence of any commercial or financial relationships that could be construed as a potential conflict of interest.

The reviewer JW declared a shared affiliation with the authors SW, XZ, PL to the handling editor at time of review.

Publisher's note

All claims expressed in this article are solely those of the authors and do not necessarily represent those of their affiliated organizations, or those of the publisher, the editors, and the reviewers. Any product that may be evaluated in this article, or claim that may be made by its manufacturer, is not guaranteed or endorsed by the publisher.

References

Anderson, T. (2002). Correction of common lead U-Pb analyses that do not report ^{204}Pb. *Chem. Geol.* 192 (1-2), 59–79. doi:10.1016/S0009-2541(02)00195-X

Antonijevic, S. K., Wagner, L. S., Kumar, A., Beck, S. L., Long, M. D., Zandt, G., et al. (2015). The role of ridges in the formation and longevity of flat slabs. *Nature* 524, 212–215. doi:10.1038/nature14648

Bach, W., Alt, J. C., Niu, Y. L., Humphris, S. E., Erzinger, J., and Dick, H. J. (2001). The geochemical consequences of late-stage low-grade alteration of lower ocean crust at the SW Indian Ridge: Results from ODP Hole 735B (Leg 176). *Geochimica Cosmochimica Acta* 65 (19), 3267–3287. doi:10.1016/s0016-7037(01)00677-9

Barbarin, B. (2005). Mafic magmatic enclaves and mafic rocks associated with some granitoids of the central sierra Nevada batholith, California: Nature, origin, and relations with the hosts. *Lithos* 80 (1-4), 155–177. doi:10.1016/j.lithos.2004.05.010

Bonin, B. (2007). A-type granites and related rocks: Evolution of a concept, problems and prospects. *Lithos* 97 (1-2), 1–29. doi:10.1016/j.lithos.2006.12.007

Breiter, K., Gardenová, N., Kanický, V., and Vaculovič, T. (2013). Gallium and germanium geochemistry during magmatic fractionation and post-magmatic alteration in different types of granitoids: A case study from the bohemian Massif (Czech republic). *Geol. Carpath.* 64, 171–180. doi:10.2478/geoca-2013-0018

Chappell, B. W., and White, A. J. R. (2001). Two contrasting granite types: 25 years later. *Aust. J. Earth Sci.* 48 (4), 489–499. doi:10.1046/j.1440-0952.2001.00882.x

Chen, H. W., Luo, Z. H., and Mo, X. X. (2005). Underplating mechanism of Triassic granite of magma mixing origin in the East Kunlun orogenic belt. *Geol. China* 32 (3), 386–395.

Chen, Z. G., Zhang, L. C., Wu, H. Y., Wan, B., and Zeng, O. D. (2008). Geochemistry study and tectonic background of A style host granite in Nianzigou molybdenum deposit in Xilamulun mollybdenum mhetallogenic belt, Inner Mongolia. *Acta Petrol. Sin.* 24 (4), 879–889.

Cheng, Y. H., Duan, L. F., Wang, S. Y., Li, Y., Teng, X. J., and Zhang, T. F. (2020). Termination of the hegenshan orogen in the xing'an-Mongolian orogenic belt, north China: Geochemical and zircon U-Pb geochronological constraints from early permian mafic dykes. *Geol. J.* 55, 845–861. doi:10.1002/gj.3463

Cheng, Y. H., Teng, X. J., Li, Y. F., Li, M., and Zhang, T. F. (2014). Early permian east-ujimqin mafic-ultramafic and granitic rocks from the xing'an-Mongolian orogenic belt, north China: Origin, chronology, and tectonic implications. *J. Asian Earth Sci.* 96 (15), 361–373. doi:10.1016/j.jseaes.2014.09.027

Clemens, J. D., Holloway, J. R., and White, J. A. R. (1986). Origin of an A-type granite; experimental constraints. *Am. Mineralogist* 71 (3), 317–324.

Deng, C. Z., Sun, D. Y., Han, J. S., Chen, H. Y., Li, G. H., Xiao, B., et al. (2019). Late-stage southwards subduction of the Mongol-Okhotsk oceanic slab and implications for porphyry Cu-Mo mineralization: Constraints from igneous rocks associated with the Fukeshan deposit, NE China. *Lithos* 326-327, 341–357. doi:10.1016/j.lithos.2018.12.030

Donskaya, T. V., Gladkochub, D. P., Mazukabzov, A. M., and Ivanov, A. V. (2013). Late Paleozoic-Mesozoic subduction related magmatism at the southern margin of the Siberian continent and the 150-million-year history of the Mongol-Okhotsk Ocean. *J. Asian Earth Sci.* 62, 79–97. doi:10.1016/j.jseaes.2012.07.023

Eby, G. N. (1992). Chemical subdivision of the A-type granitoids: Petrogenetic and tectonic implications. *Geology* 20 (7), 641. doi:10.1130/0091-7613(1992)020<0641:csotat>2.3.co;2

Frost, B. R., and Frost, C. D. (2008). A geochemical classification for feldspathic igneous rocks. *J. Petrology* 49 (11), 1955–1969. doi:10.1093/petrology/egn054

Gao, S., Chen, W. F., Hu, J., Xie, G. A., and Ling, H. F. (2022). A Late Jurassic A-type granitic-magmatic belt in the westernmost Northeast China and its tectonic implications. *Tectonophysics* 834, 229339. doi:10.1016/j.tecto.2022.229339

Gao, S., Chen, W. F., Ling, H. F., Sun, L. Q., Ren, Q., Xie, G. A., et al. (2021). A latest jurassic A-type granite in the middle of inner Mongolia: Petrogenesis and tectonic implications. *Lithos* 394-395, 106167. doi:10.1016/j.lithos.2021.106167

Gillespie, J., Glorie, S., Xiao, W. J., Zhang, Z. Y., Collins, A. S., Evans, N., et al. (2017). Mesozoic reactivation of the beishan, southern central asian orogenic belt: Insights from low-temperature thermochronology. *Gondwana Res.* 43, 107–122. doi:10.1016/j.gr.2015.10.004

Griffin, W. L., Wang, X., Jackson, S. E., Pearson, N. J., O'Reilly, S. Y., Xu, X. S., et al. (2002). Zircon chemistry and magma mixing, SE China: *In-situ* analysis of Hf isotopes, tonglu and pingtan igneous complexes. *Lithos* 61 (3-4), 237–269. doi:10.1016/s0024-4937(02)00082-8

Hart, S. R., Blusztajn, J., Dick, H. J., Meyer, P. S., and Muehlenbachs, K. (1999). The fingerprint of seawater circulation in a 500-meter section of ocean crust gabbros. *Geochimica Cosmochimica Acta* 63 (23), 4059–4080. doi:10.1016/s0016-7037(99)00309-9

Holland, T., and Blundy, J. (1994). Non-ideal interactions in calcic amphiboles and their bearing on amphibole-plagioclase thermometry. *Contributions Mineralogy Petrology* 116, 433–447. doi:10.1007/bf00310910

Hoskin, P. W., and Schaltegger, U. (2003). The composition of zircon and igneous and metamorphic petrogenesis. *Rev. Mineralogy Geochem.* 53 (1), 27–62. doi:10.2113/0530027

Jahn, B. M., Griffin, W. L., and Windley, B. F. (2000). Continental growth in the phanerozoic: Evidence from central asia. *Tectonophysics* 328, 1–227. doi:10.1016/s0040-1951(00)00174-8

Ji, Z., Meng, Q. A., Wan, C. B., Zhu, D. F., Ge, W. C., Zhang, Y. L., et al. (2019). Geodynamic evolution of flat-slab subduction of Paleo-Pacific plate: Constraints from jurassic adakitic lavas in the Hailar Basin, NE China. *Tectonics* 38 (12), 4301–4319. doi:10.1029/2019tc005687

Jian, P., Liu, D. Y., Kroner, A., Windley, B. F., Shi, Y. R., Zhang, W., et al. (2010). Evolution of a permian intraoceanic arc-trench system in the solonker suture zone, central asian orogenic belt, China and Mongolia. *Lithos* 118 (1), 169–190. doi:10.1016/j.lithos.2010.04.014

Jiang, X. J., Peng, Y. B., Dong, X. J., Li, H. M., and Tu, Y. (2021). The remote role of Mongolia-okhotsk ocean: Evidences from the origin of rhyolite porphyry in yangpangou area, the southeast of inner Mongolia. *Earth Sci.* 46 (9), 3057–3073. doi:10.3799/dqkx.2020.335

Jin, S. (2020). Study of material composition and tectonic properties of the Duerji tectonic melange, Inner Mongolia. *Acta Geol. Sin.* 94 (8), 2227–2242. doi:10.19762/j.cnki.dizhixuebao.2020062

King, P. L., Chappell, B. W., Allen, C. M., and White, A. J. R. (2001). Are A-type granites the high-temperature felsic granites? Evidence from fractionated granites of the wangrah suite. *Aust. J. Earth Sci.* 48, 501–514. doi:10.1046/j.1440-0952.2001.00881.x

Lee, C. T. A., and Bachmann, O. (2014). How important is the role of crystal fractionation in making intermediate magmas? Insights from Zr and P systematic. *Earth Planet. Sci. Lett.* 393, 266–274. doi:10.1016/j.epsl.2014.02.044

Li, W. P. (2012). Magma evolution of the late jurassic volcanic rocks and its Genesis of the langi formation, beipiao area, Western liaoning province. *Earth Sci.* 37 (1), 47–56. doi:10.3799/dqkx.2012.005

Li, Y. J., Wang, G. H., Santosh, M., Wang, J. F., Dong, P. P., and Li, H. Y. (2020). Subduction initiation of the SE Paleo-Asian Ocean: Evidence from a well preserved intra-oceanic forearc ophiolite fragment in central Inner Mongolia, North China. *Earth Planet. Sci. Lett.* 535, 116087. doi:10.1016/j.epsl.2020.116087

Li, Y. J., Wang, G. H., Santosh, M., Wang, J. F., Dong, P. P., and Li, H. Y. (2018b). Supra-subduction zone ophiolites from inner Mongolia, north China: Implications for the tectonic history of the southeastern central asian orogenic belt. *Gondwana Res.* 59, 126–143. doi:10.1016/j.gr.2018.02.018

Li, Y., Xu, W. L., Tang, J., Pei, F. P., Wang, F., and Sun, C. Y. (2018a). Geochronology and geochemistry of Mesozoic intrusive rocks in the Xing'an Massif of NE China: Implications for the evolution and spatial extent of the Mongol-Okhotsk tectonic regime. *Lithos* 304-307, 57–73. doi:10.1016/j.lithos.2018.02.001

Liu, C. S., Chen, X. M., Chen, P. R., Wang, R. C., and Hu, H. (2003). Subdivision, discrimination criteria and Genesis for A type rock suites. *Geol. J. China Univ.* 9 (4), 573–591. doi:10.16108/j.issn1006-7493.2003.04.011

Liu, H. D., Cheng, Y. H., Santosh, M., Teng, X. M., Zhang, X. W., and Teng, X. J. (2021). Magmatism associated with lithospheric thinning, mantle upwelling, and extensional tectonics: Evidence from Carboniferous-Permian dyke swarms and granitoids from Inner Mongolia, Central Asian Orogenic Belt. *Lithos* 386-387, 106004. doi:10.1016/j.lithos.2021.106004

Liu, W., Siebel, W., Li, X. J., and Pan, X. F. (2005). Petrogenesis of the Linxi granitoids, northern Inner Mongolia of China: Constraints on basaltic underplating. *Chem. Geol.* 219 (1-4), 5–35. doi:10.1016/j.chemgeo.2005.01.013

Liu, Y. J., Li, W. M., Feng, Z. Q., Wen, Q. B., Neubauer, F., and Liang, C. Y. (2017). A review of the paleozoic tectonics in the eastern part of central asian orogenic belt. *Gondwana Res.* 43, 123–148. doi:10.1016/j.gr.2016.03.013

Liu, Y. S., Hu, Z. C., Gao, S., Günther, D., Xu, J., Gao, C. G., et al. (2008). *In situ* analysis of major and trace elements of anhydrous minerals by LA-ICP-MS without applying an internal standard. *Chem. Geol.* 257 (1), 34–43. doi:10.1016/j.chemgeo.2008.08.004

Loiselle, M. C., and Wones, D. R. (1979). Characteristics and origin of anorogenic granites. *Geol. soc. am. abstr. Progr* 11, 468.

Maniar, P. D., and Piccoli, P. M. (1989). Tectonic discrimination of granitoids. *Geol. Soc. Am. Bull.* 101, 635–643. doi:10.1130/0016-7606(1989)101<0635:tdog>2.3.co;2

Meng, E., Xu, W. L., Yang, D. B., Qiu, K. F., Li, C. H., and Zhu, H. T. (2011). Zircon U-Pb chronology, geochemistry of Mesozoic volcanic rocks from the Lingquan Basin in Manzhouli area, and its tectonic implications. *Acta Petrol. Sin.* 27 (4), 1209–1226.

Meng, Q. R., Wu, G. L., Fan, L. G., Wei, H. H., and Wang, E. (2020). Late Triassic uplift, magmatism and extension of the northern North China block: Mantle signatures in the surface. *Earth Planet. Sci. Lett.* 547, 116451. doi:10.1016/j.epsl.2020.116451

Miao, L. C., Fan, W. M., Liu, D. Y., Shi, Y. R., and Guo, F. (2008). Geochronology and geochemistry of the Hegenshan ophiolitic complex: Implications for late-stage tectonic evolution of the Inner Mongolia-Daxinganling Orogenic Belt, China. *J. Asian Earth Sci.* 32 (5-6), 348–370. doi:10.1016/j.jseaes.2007.11.005

Nozaka, T., and Liu, Y. (2002). Petrology of the Hegenshan ophiolite and its implication for the tectonic evolution of northern China. *Earth Planet. Sci. Lett.* 202 (1), 89–104. doi:10.1016/s0012-821x(02)00774-4

Parfenov, L. M., Popeko, L. I., and Tomurtogoo, O. (2001). Problems of tectonics of the mongol-okhotsk orogenic belt. *Geol. Pac. Ocean* 16 (5), 797–830.

Pearce, J. A. (1996). Sources and settings of granitic rocks. *Episodes* 19, 120–125. doi:10.18814/epiiugs/1996/v19i4/005

Peng, Y. D., Huang, F., Xing, D. H., and Lv, A. C. (2012). Geochemical characteristics and tectonic setting for volcanic rocks of Zhangjiakou Formation in the Chaoyang area,'Western Liaoning. *J. Northeast. Univ. Nat. Sci.* 33 (9), 1331–1335. doi:10.1007/s11783-011-0280-z

Pérez-Soba, C., and Villaseca, C. (2010). Petrogenesis of highly fractionated I-type peraluminous granites: La pedriza pluton (Spanish central system). *Geol. Acta* 8, 131–149. doi:10.1344/105.000001527

Rajesh, H. M. (2000). Characterization and origin of a compositionally zoned aluminous A-type granite from South India. *Geol. Mag.* 137, 291–318. doi:10.1017/s001675680000399x

Rapp, R. P., and Watson, E. B. (1995). Dehydration melting of metabasalt at 8-32kbar: Implications for continental growth and crust-mantle recycling. *J. Petrology* 36 (4), 891–931. doi:10.1093/petrology/36.4.891

Safonova, I., Kotlyarov, A., Krivonogov, S., and Xiao, W. J. (2017). Intra-oceanic arcs of the Paleo-Asian ocean. *Gondwana Res.* 50 (3), 167–194. doi:10.1016/j.gr.2017.04.005

Shao, J. A., Tian, W., Tang, K. D., and Wang, Y. (2015). Petrogenesis and tectonic settings of the late carboniferous high M basalts of inner Mongolia. *Earth Sci. Front.* 22 (5), 171–181. doi:10.13745/j.esf.2015.05.014

Shi, Y. R., Liu, C., Deng, J. F., and Jian, P. (2014). Geochronological frame of granitoids from Central Inner Mongolia and its tectonomagmatic evolution. *Acta Petrol. Sin.* 30 (11), 3155–3171.

Sisson, T. W., Ratajeski, K., Hankins, W. B., and Glazner, A. F. (2005). Voluminous granitic magmas from common basaltic sources. *Contributions Mineralogy Petrology* 148 (6), 635–661. doi:10.1007/s00410-004-0632-9

Sun, S. S., and McDonough, W. F. (1989). Chemical and isotopic systematics of oceanic basalts: Implications for mantle composition and processes. *Geol. Soc. Lond. Special Publ.* 42, 313–340.

Tang, J., Xu, W. L., Wang, F., Zhao, S., and Li, Y. (2015). Geochronology, geochemistry, and deformation history of Late Jurassic-Early Cretaceous intrusive rocks in the Erguna Massif, NE China: Constraints on the late Mesozoic tectonic evolution of the Mongol-Okhotsk orogenic belt. *Tectonophysics* 658, 91–110. doi:10.1016/j.tecto.2015.07.012

Turner, S. P., Foden, J. D., and Morrison, R. S. (1992). Derivation of some A-type magmas by fractionation of basaltic magma: An example from the padthaway ridge, south Australia. *Lithos* 28 (2), 151–179. doi:10.1016/0024-4937(92)90029-x

Wang, F., Zhou, X. H., Zhang, L. C., Ying, J. F., Zhang, Y. T., Wu, F. Y., et al. (2006). Late mesozoic volcanism in the Great xing'an range (NE China): Timing and implications for the dynamic setting of NE asia. *Earth Planet. Sci. Lett.* 251 (1-2), 179–198. doi:10.1016/j.epsl.2006.09.007

Wang, J. G., He, Z. H., and Xu, W. L. (2013). Petrogenesis of riebeckite rhyolites in the southern Da Hinggan Mts: Geohronological and geochemical evidence. *Acta Petrol. Sin.* 29 (3), 853–863.

Wang, T., Guo, L., Zhang, L., Yang, Q. D., Zhang, J. J., Tong, Y., et al. (2015). Timing and evolution of jurassic-cretaceous granitoid magmatisms in the mongol-okhotsk belt and adjacent areas, NE asia: Implications for transition from contractional crustal thickening to extensional thinning and geodynamic settings. *J. Asian Earth Sci.* 97 (1), 365–392. doi:10.1016/j.jseaes.2014.10.005

Wang, T., Tong, Y., Zhang, L., Li, S., Huang, H., Zhang, J. J., et al. (2017). Phanerozoic granitoids in the central and eastern parts of Central Asia and their tectonic significance. *J. Asian Earth Sci.* 145, 368–392. doi:10.1016/j.jseaes.2017.06.029

Watson, E. B. (1979). Zircon saturation in felsic liquids: Experimental results and applications to trace element geochemistry. *Contributions Mineralogy Petrology* 70 (4), 407–419. doi:10.1007/bf00371047

Whalen, J. B., Currie, K. L., and Chappell, B. W. (1987). A-Type granites: Geochemical characteristics, discrimination and petrogenesis. *Contributions Mineralogy Petrology* 95 (4), 407–419. doi:10.1007/bf00402202

Whitney, J. A., and Stormer, J. C. (1985). Mineralogy, petrology, and magmatic conditions from the fish canyon tuff, central san juan volcanic field, Colorado. *J. Petrology* 26, 726–762. doi:10.1093/petrology/26.3.726

Windley, B. F., Alexeiev, D., Xiao, W. J., Kroner, A., and Badarch, G. (2007). Tectonic models for accretion of the central asian orogenic belt. *J. Geol. Soc.* 164 (1), 31–47. doi:10.1144/0016-76492006-022

Wu, F. Y., Liu, X. C., Ji, W. Q., Wang, J. M., and Yang, L. (2017). Highly fractionated granites: Recognition and research. *Sci. China Earth Sci.* 7, 1201–1219. doi:10.1007/s11430-016-5139-1

Wu, F. Y., Sun, D. Y., Ge, W. C., Zhang, Y. B., Grant, M. L., Wilde, S. A., et al. (2011). Geochronology of the Phanerozoic granitoids in northeastern China. *J. Asian Earth Sci.* 41 (1), 1–30. doi:10.1016/j.jseaes.2010.11.014

Wu, F. Y., Sun, D. Y., Li, H., Jahn, B. M., and Wilde, S. A. (2002). A-type granites in northeastern China: Age and geochemical constraints on their petrogenesis. *Chem. Geol.* 187 (1-2), 143–173. doi:10.1016/s0009-2541(02)00018-9

Wu, F. Y., Yang, J. H., Wilde, S. A., and Zhang, X. O. (2005). Geochronology, petrogenesis and tectonic implications of Jurassic granites in the Liaodong Peninsula, NE China. *Chem. Geol.* 221 (1), 127–156. doi:10.1016/j.chemgeo.2005.04.010

Wu, S. P., Wang, M. Y., and Qi, K. J. (2007). Present situation of researches on A-type granites: A revie. *Acta Petrologica Mineralogica* 26 (1), 57–66. doi:10.3969/j.issn.1009-2374.2007.08.079

Xiao, W. J., Windley, B. F., Hao, J. J., and Zhai, M. G. (2003). Accretion leading to collision and the Permian Solonker suture, Inner Mongolia, China: Termination of the central Asian orogenic belt. *Tectonics* 22 (6), 1069. doi:10.1029/2002tc001484

Xie, H. J., Wu, G., Zhu, M. T., Liu, J., and Zhang, L. C. (2012). Geochronology and geochemistry of the Daolanghuduge A-type granite in Inner Mongolia, and its geological significance. *Acta Petrol. Sin.* 28 (2), 483–494.

Xu, B., Zhao, P., Bao, Q. Z., Zhou, Y. H., Wang, Y. Y., and Luo, Z. W. (2014). Preliminary study on the pre-Mesozoic tectonic unit division of the Xing-Meng Orogenic Belt (XMOB). *Acta Petrol. Sin.* 30 (7), 1841–1857.

Xu, M. J., Xu, W. L., Meng, E., and Wang, F. (2011). LA-ICP-MS zircon U-Pb chronology and geochemistry of Mesozoic volcanic rocks from the Shanghulin-Xiangyang Basin in Ergun area, northeastern Inner Mongolia. *Geol. Bull. China* 30 (9), 1321–1338. doi:10.3969/j.issn.1671-2552.2011.09.001

Xu, W. L., Wang, F., Pei, F. P., Meng, E., Tang, J., Xu, M. J., et al. (2013). Mesozoic tectonic regimes and regional ore-forming background in NE China: Constraints from spatial and temporal variations of Mesozoic volcanic rock associations. *Acta Petrol. Sin.* 29 (2), 339–353.

Xue, F. H., Zhang, X. H., Deng, J. X., and Yuan, L. L. (2015). Late Jurassic A-type granite from the Dalai region of central Inner Mongolia: Geochemistry, petrogenesis and tectonic implication. *Acta Petrol. Sin.* 31 (6), 1774–1788.

Yang, Q. D., Guo, L., Wang, T., Zeng, T., Zhang, L., Tong, Y., et al. (2014). Geochronology, origin, sources and tectonic settings of Late Mesozoic two-stage granites in the Ganzhuermiao region, central and southern Da Hinggan Range, NE China. *Acta Petrol. Sin.* 30 (7), 1961–1981.

Zhang, C., Quan, J. Y., Zhang, Y. J., Liu, Z. H., Li, W., Wang, Y., et al. (2020). Late Mesozoic tectonic evolution of the southern Great Xing'an Range, NE China: Evidence from whole-rock geochemistry, and zircon U-Pb ages and Hf isotopes from volcanic rocks. *Lithos* 362-363, 105409. doi:10.1016/j.lithos.2020.105409

Zhang, J. H., Gao, S., Ge, W. C., Wu, F. Y., Yang, J. H., Wilde, S. A., et al. (2010). Geochronology of the mesozoic volcanic rocks in the Great xing'an range, northeastern China: Implications for subduction-induced delamination. *Chem. Geol.* 276, 144–165. doi:10.1016/j.chemgeo.2010.05.013

Zhang, J. H., Ge, W. C., Wu, F. Y., Wilde, S. A., Yang, J. H., and Liu, X. M. (2008). Large-scale early cretaceous volcanic events in the northern Great xing'an range, northeastern China. *Lithos* 102 (1-2), 138–157. doi:10.1016/j.lithos.2007.08.011

Zhang, Q., Ran, H., and Li, C. D. (2012). A-type granite: What is the essence? *Acta Petrologica Mineralogica* 31 (4), 621–626.

Zhang, S. H., Zhao, Y., Davis, G. A., Ye, H., and Wu, F. (2014). Temporal and spatial variations of mesozoic magmatism and deformation in the North China craton: Implications for lithospheric thinning and decratonization. *Earth Sci. Rev.* 131, 49–87. doi:10.1016/j.earscirev.2013.12.004

Zhang, S. H., Zhao, Y., Liu, X. C., Liu, D. Y., Chen, F. K., Xie, L. W., et al. (2009a). Late paleozoic to early mesozoic mafic–ultramafic complexes from the northern North China block: Constraints on the composition and evolution of the lithospheric mantle. *Lithos* 110 (1-4), 229–246. doi:10.1016/j.lithos.2009.01.008

Zhang, S. H., Zhao, Y., Song, B., Hu, J. M., Liu, S. W., Yang, Y. H., et al. (2009b). Contrasting late carboniferous and late permian–middle triassic intrusive suites from the northern margin of the North China craton: Geochronology, petrogenesis, and tectonic implications. *Geol. Soc. Am. Bull.* 121 (1-2), 181–200. doi:10.1130/b26157.1

Zhang, Y. T., Sun, F. Y., Wang, S., and Wei, X. (2018). Geochronology and geochemistry of late jurassic to early cretaceous granitoids in the northern Great xing'an range, NE China: Petrogenesis and implications for late mesozoic tectonic evolution. *Lithos* 312-313, 171–185. doi:10.1016/j.lithos.2018.05.006

Zheng, Y. D., Davis, G. A., Wang, C., Darby, B. J., and Zhang, C. H. (2000). Major mesozoic tectonic events in the yanshan belt and the plate tectonic setting. *Acta Geol. Sin.* 19 (4), 289–302. doi:10.3321/j.issn:0001-5717.2000.04.001

Zhou, J. B., Han, J., Zhao, G. C., Zhang, X. Z., Cao, J. L., Wang, B., et al. (2015a). The emplacement time of the Hegenshan ophiolite: Constraints from the unconformably overlying Paleozoic strata. *Tectonophysics* 662, 398–415. doi:10.1016/j.tecto.2015.03.008

Zhou, Z. H., Lv, L. S., Yang, Y. J., and Li, T. (2010). Petrogenesis of the early cretaceous A-type granite in the huanggang Sn-Fe deposit, inner Mongolia: Constraints from zircon U-Pb dating and geochemistry. *Acta Petrol. Sin.* 26 (12), 3521–3537.

Zhu, H. T., Wu, J. H., Tang, D. W., Guo, H. F., Yang, D. G., Wang, L. Y., et al. (2020). Geochemistry of late jurassic biotite granite in the hongshanzi area, hexigten banner, inner Mongolia, and its geological implications. *Acta Geol. Sin.* 66 (3), 765–785. doi:10.16509/j.georeview.2020.03.017

Zhu, R., and Xu, Y. (2019). The subduction of the west Pacifific plate and the destruction of the North China Craton. *Sci. China Earth Sci.* 9, 1340–1350. doi:10.1007/s11430-018-9356-y

Zorin, Y. A. (1999). Geodynamics of the Western part of the Mongolia-okhotsk collisional belt, trans-baikal region (Russia) and Mongolia. *Tectonophysics* 306 (1), 33–56. doi:10.1016/s0040-1951(99)00042-6